THE JOURNAL OF PHYSICAL CHEMISTRY C

Article

pubs.acs.org/JPCC

SBR/$BiFeO_3$ Elastomer Capacitor Films Prepared under Magnetic and Electric Fields Displaying Magnetoelectric Coupling

Leila María Saleh Medina,[†] Guillermo A. Jorge,[§] Diego Rubi,[∥,⊥] Norma D'Accorso,[‡] and R. Martín Negri*[,†]

[†]Instituto de Química Física de Materiales, Ambiente y Energía (INQUIMAE), Departamento de Química Inorgánica, Analítica y Química Física, Facultad de Ciencias Exactas y Naturales, and [‡]Centro de Investigación en Hidratos de Carbono (CIHIDECAR, CONICET-UBA), Departamento de Química Orgánica, Facultad de Ciencias Exactas y Naturales, Universidad de Buenos Aires, Buenos Aires, Argentina

[§]Instituto de Ciencias, Universidad Nacional de General Sarmiento, Buenos Aires, Argentina

[∥]Gerencia de Investigación y Aplicaciones, Centro Atómico Constituyentes, Comisión Nacional de Energía, Atómica, Argentina

[⊥]Escuela de Ciencia y Tecnología, Universidad Nacional de San Martín, Campus Miguelete, San Martín, Buenos Aires, Argentina

ABSTRACT: The dielectric properties of elastomer composites formed by dispersions of bismuth ferrite ($BiFeO_3$) multiferroic filler particles in styrene−butadiene rubber (SBR) were studied. The SBR/$BiFeO_3$ films (10−100 μm) were prepared in the presence of electric (E) or magnetic fields (H), showing remarkable characteristics in comparison with systems obtained in its absence. The dispersed multiferroic fillers form clusters of much smaller size when prepared under E or H. The dielectric constant, ε (measured up to 1 MHz), increases with $BiFeO_3$ concentration until reaching saturation. The rise of ε was obtained at concentrations much lower for samples prepared in the presence of E or H than in its absence. Saturation is assigned to connectivity between filler clusters at the largest concentrations, increasing leakage currents and limiting the dielectric behavior. The whole dependence of ε with $BiFeO_3$ concentration was described using a proposed model. The dc resistivities, ρ, increase with $BiFeO_3$ concentration but remain high ($\rho \approx 10$ GΩ·cm), allowing using the films as capacitors with filter action between 100 kHz and 7 MHz. The films prepared in the presence of H present strong dependence of the ferroelectric response with magnetic fields applied *after* preparation; that is, electromagnetic coupling was observed in those samples.

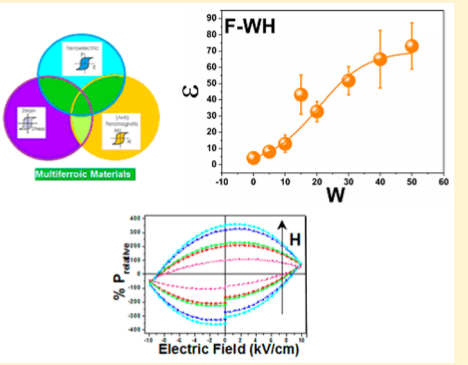

1. INTRODUCTION

Elastomer composites formed by dispersions of inorganic fillers in an organic elastomer polymer are receiving increasing attention for their applications in flexible circuits, magneto-rheological systems, and sensors.[1−5] Of central relevance are the possibilities of choosing the organic matrix and inorganic filler according to the specific application. For instance, electrically conductive fillers and elastomer polymers are broadly used for pressure sensors, where random dispersions of particles may present strain-dependent electrical conduction.[6] Alternatives to randomly dispersed systems are the *structured* composites, where the inorganic fillers are oriented inside the organic matrix by applying an external field during preparation. The structured composites present anisotropic properties, such as anisotropic electric piezoresistivity, magnetoresistance, or magnetoelasticity. We have developed anisotropic pressure and magnetic sensors by dispersing magnetic nanoparticles coated with silver (to obtain electrical conduction) in polydimethysiloxane (PDMS) by applying a uniform magnetic field while curing.[3,7,8] Recently, we obtained structured submillimeter films of styrene−butadiene−rubber (SBR) embedded with Fe_3O_4−Ag superparamagnetic particles by evaporating the solvent between two magnets. The particles group forming needle-like structures aligned in the direction of the magnetic field applied during preparation, providing the anisotropic properties. The concentration threshold for obtaining the desired effect is significantly reduced in comparison with random composites.[9]

Other devices of high relevance are elastomer/multiferroic capacitors, where a multiferroic filler, which presents simultaneously magnetic and electric orders at room temperature,[10,11] is dispersed in the elastomer polymer. The exploration of these systems has already been started recently using $BiFeO_3$ nanoparticles, which are the paradigmatic single-phase multiferroic compounds.[12−16] For instance, Bhadra et al.[13] used the ferroelectric elastomer poly(vinylidene fluoride) (PVDF), whose dielectric response was enhanced by randomly dispersing $BiFeO_3$. Tamboli et al. and Ahlawat et al. reported

Received: June 24, 2015
Revised: September 16, 2015

DOI: 10.1021/acs.jpcc.5b06056
J. Phys. Chem. C XXXX, XXX, XXX−XXX

on the dielectric properties of random dispersions of $BiFeO_3$ but in nonelastomer polymers.[14,15] These studies remark on the high potentiality of polymer/$BiFeO_3$ systems.

In the present work we investigate the capacitive response of films based on the elastomer polymer styrene−butadiene−rubber (SBR) containing dispersed $BiFeO_3$ nanoparticles, preparing the composite in the presence of uniform electric or magnetic fields. Note that the polymer matrix is not a ferroelectric, as in the case of PVDF. We show here that as filler concentration increases, the films start to present capacitive response to ac stimulus. Additionally, we observed that the ferroelectric response of those films is influenced by other external magnetic fields (magnetoelectric coupling). Thus, the aims of the present work are to analyze the characteristics of elastomer/$BiFeO_3$ films as capacitors, using a nonferroelectric polymer (SBR), preparing the composites in the presence of external fields, and to investigate the magnetoelectric coupling effects.

2. EXPERIMENTAL SECTION

In a previous work we describe the synthesis and characterization of $BiFeO_3$ ceramic particles by acid−base coprecipitation.[17] The same procedure was followed to synthesize the samples used in this work. Characterization studies included X-ray diffraction (XRD), differential scanning calorimetry (DSC), Fourier transform infrared (FTIR), scanning electron microscopy (SEM), and energy dispersive spectroscopy (EDS). The description of these instrumental facilities was presented in the previous work.[17]

Commercial styrene−butadiene−rubber, referred to as SBR, was provided by FATE S.A.I.C.I. (Argentina). Gel permeation chromatography (SEC) analysis led to $M_w \approx 390\,000$. The styrene:butadiene ratio, determined by ^1H NMR, was determined about 23.5:76.5 with 2% w/w of carboxylated additives.[9,18]

Elastomeric composites were prepared by adding different amounts of $BiFeO_3$ ceramics to a solution of SBR in toluene. The viscous suspension was deposited by spin-coating onto silicon wafers (n-Si), obtaining nondried composite films. Then solvent was left to evaporate at room temperature and under the application of magnetic or electric fields. The fields were applied perpendicular to the surface of the substrate. In the case of magnetic alignment the films formed on the substrate were placed between two rare earth permanent magnets (disk shaped, flat surfaces, 36 mm diameter) immediately after the spin-coating process, and the system was left between the magnets at room temperature until toluene was completely evaporated. The magnetic field between the two magnets, close to the surface of the film and at its center, $\mu_0 H$, was measured with a Hall-probe sensor (Allegro Probe Model 1302A) and estimated about 360 mT. In the case of the electric field, a fixed voltage (99 V) was applied trough the spin-coated films providing electric fields, E, in the range of 10−100 kV/cm, depending on the thickness of each sample. After complete solvent evaporation, the top surface of the films was coated with a silver layer to improve the electrical contact. The area of the top electrodes used to measure the dielectric properties, a, was 0.01 cm^2 in all cases.

The thicknesses of the different films (after solvent evaporation) were measured using a surface profilometer (Veeco, model Dektak 150). Samples are placed on a glass microscope slide, and the stage moves the films beneath a diamond-tipped stylus, scanning the surface at a programmed scanning rate (75 $\mu m\ s^{-1}$ was used). The stylus is linked to a linear variable differential transformer (LDVT) which produces and processes electrical signals assigned to surface variations. The measurements were performed in different regions of the films, scanning the samples until reaching its edge. In this way, the thickness of the film, L, was measured as a function of the scanned distance. A typical range for the total distance scanned by the probe was 3000 μm. This range includes scanning a broad region of the substrate (500−700 μm depending on the sample) in order to define a flat baseline. Average values of L, referred as $\langle L \rangle$, were calculated within a defined scanning distance range (500−1500 μm, depending on the sample) starting from at least 100 μm since the edge of the film.

The structure of the dried composite films was investigated by SEM using a field emission scanning electron microscope (FESEM; Zeiss Supra 40 Gemini) and by atomic force microscopy (AFM) using an AFM-STM DI-VEECO MMAFM NANOSCOPE IIIA device. Intermittent mode was used to take topographic images of the samples (areas of 20 μm × 20 μm were sampling).

Impedance analysis was carried on a TEQ 4 potentiostat (Argentina) for frequencies, f, between 0.1 Hz and 1 MHz. Additionally, the capacitive behavior in an expanded frequency range (f between 100 kHz and 7 MHz) was studied by analyzing the response of the samples in series with a 1 kΩ commercial resistance to a sinusoidal wave generated with a Siglent SDG 1050 generator. The response of the circuit was determined with a Hantek MS05062D dual-channel oscilloscope (60 MHz broadband). The oscilloscope probes used at the test points were previously calibrated against a square-waveform internal reference signal by adjusting the probe's capacitance until obtaining input signals that match almost exactly the reference waveform, thus minimizing probing effects.

The ferroelectric characterization was performed using a Precision LC Material Analyzer (Radiant Technologies). Polarization curves (P−E curves) were taken at a rate of 1562.5 Hz by applying a bipolar triangular wave (0; $+V_{max}$; $-V_{max}$; 0). Density current plots of dc currents (J−E plots) were recorded with the LC analyzer. In these cases the bottom electrode, n-Si, was connected to ground.

The effect of an external magnetic field on the dielectric properties (electromagnetic coupling) was determined by inserting the sample between the pole pieces (10 cm diameter) of a Varian low impedance electromagnet (model V3703). These kinds of electromagnets are known to provide highly homogeneous steady magnetic fields, H (expressed in Oe), that were measured with a Group3 DTM-133 digital teslameter. A specially designed setup was implemented in order to place the samples between the electromagnet and to provide the electrical contacts for establishing communication with the Precision LC Material Analyzer. In this way it was possible to register P−E curves simultaneously with the application of a given magnetic field H, whose value can be arbitrarily fixed.

3. RESULTS AND DISCUSSION

3.1. Morphological Characterization of the Films. The samples are named taking into account the application or not of magnetic and electric fields during preparation (H and E, respectively) and the relative mass fraction of $BiFeO_3$ with respect to the mass of SBR multiplied by 100, referred as W ($W \equiv 100 \cdot M_{BiFeO_3}/M_{SBR}$), as illustrated in Table 1.

DOI: 10.1021/acs.jpcc.5b06056
J. Phys. Chem. C XXXX, XXX, XXX−XXX

Table 1. Nomenclature of the Films

film code	$W \equiv 100 \cdot M_{BiFeO_3}/M_{SBR}$	external field applied during preparation
F-W	W	none
F-WE	W	electric field (E)
F-WH	W	magnetic field (H)

The average thicknesses of the films ($\langle L \rangle$) are in the range of 10−100 μm, determined by profilometry for each sample. The areas (A) are about 0.5 cm^2 (depending on the sample), determined by SEM and optical microscopy. These areas are larger than the top electrode area (a = 0.01 cm^2 as indicated in the previous section). No relevant differences or trends in $\langle L \rangle$ or A for samples prepared in the absence and presence of H or E were observed.

SEM micrographs of films **F-50**, **F-50E**, and **F-50H** are shown in Figure 1 (with different magnifications). The shiny white points (agglomerations of $BiFeO_3$ particles) are uniformly distributed in the SBR matrix when either fields E or H are applied during solvent evaporation (Figure 1c−f). In contrast, if no fields are applied during preparation, the particles form larger agglomerates (Figure 1a,b).

AFM images of films **F-10** and **F-10H** are illustrated in Figure 2.

In the case of the sample shown in Figure 1, each shiny point has an average area of 6 ± 5 μm^2 (**F-50**), 0.26 ± 0.10 μm^2 (**F-50E**), and 0.30 ± 0.10 μm^2 (**F-50H**), which clearly illustrate the filler dispersion. The density of those shiny white points in the matrix are 0.04, 1.86, and 2.10 μm^{-2} for **F-50**, **F-50E**, and **F-50H**, respectively, showing that the areal density of agglomerates is higher when external fields are applied. These results show that preparation in the presence of external fields induces a finer dispersion of ceramic agglomerates. A reasonable hypothesis for this behavior is that $BiFeO_3$ particles follow the field lines when the solvent is still present, a process that seems to limit the aggregation of $BiFeO_3$ particles.

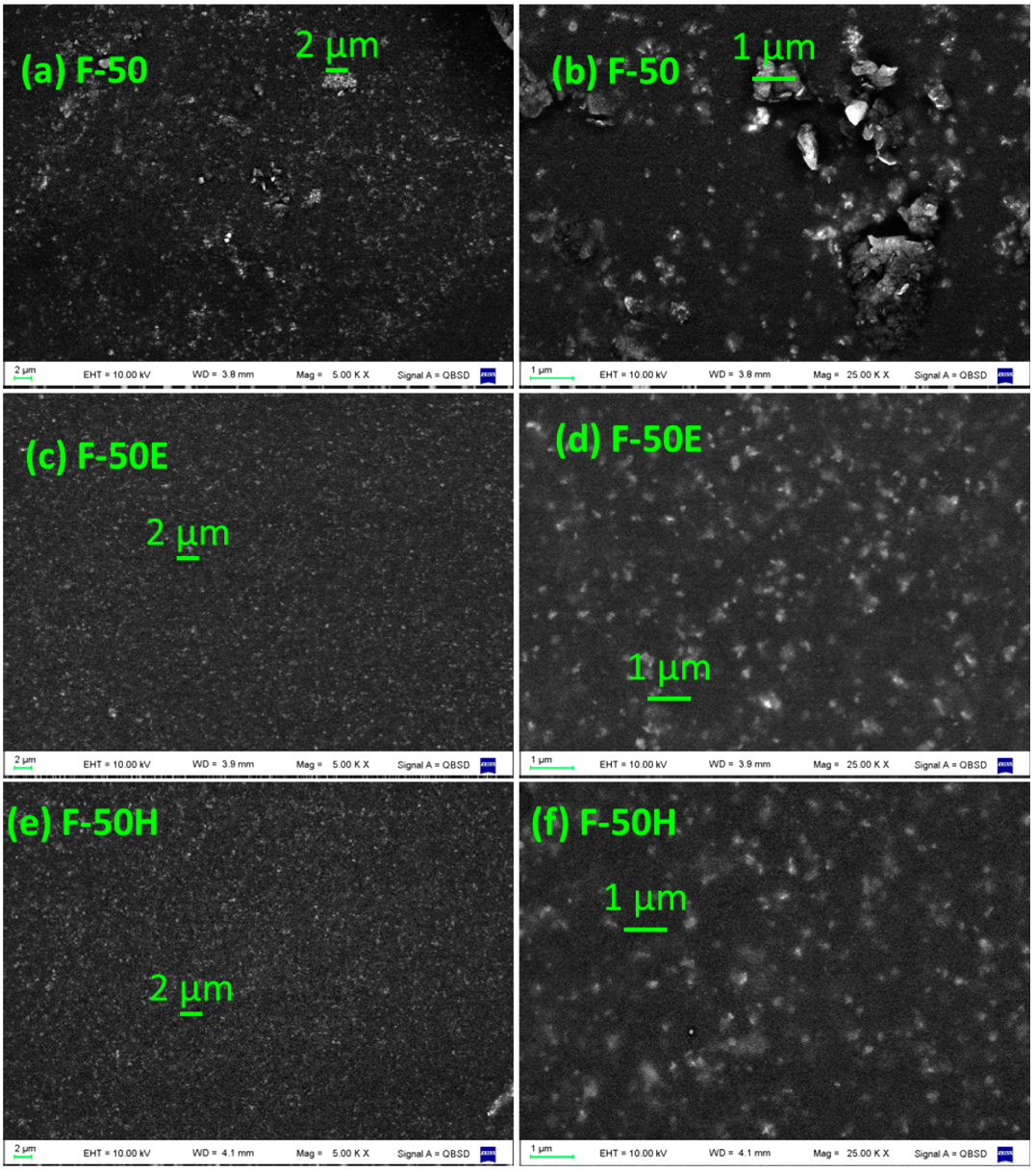

Figure 1. Top view (SEM) of SBR/$BiFeO_3$ films.

DOI: 10.1021/acs.jpcc.5b06056
J. Phys. Chem. C XXXX, XXX, XXX−XXX

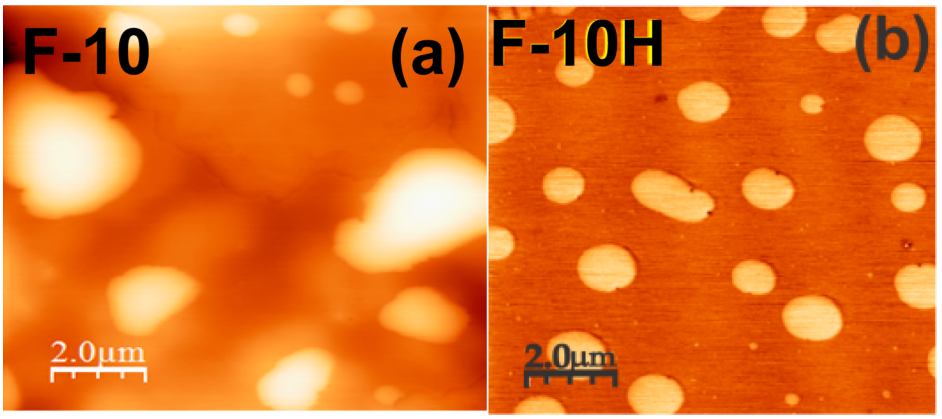

Figure 2. AFM images of (a) **F-10** and (b) **F-10H**.

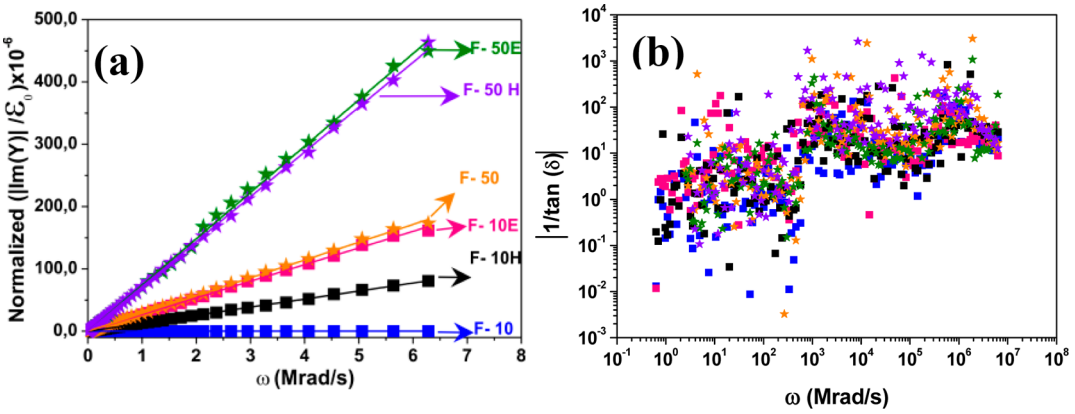

Figure 3. (a) The ordinate represents $10^{-6}|Y|/(\varepsilon_0 a/\langle L\rangle)$ which is plotted as a function of $\omega = 2\pi f$. (b) A log−log plot of $|(\tan(\delta)^{-1})|$ as a function of $\omega = 2\pi f$. Blue square, **F- 10**; magenta square, **F-10E**; black square, **F-10H**, yellow star, **F-50**; green star, **F-50E**; purple star, **F-50H**.

It is important to remark that formation of highly ordered structures, such as macroscopic (mm) pseudochains oriented in the direction of the fields were not observed. These kind of macroscopic structures were previously observed only in the case of fillers such as $CoFe_2O_4$, Fe_3O_4, or $BaTiO_3$, which present very much stronger magnetic and electric response than the $BiFeO_3$ ceramics described here.

3.2. Dielectric Characterization. The response of the films to an ac sinusoidal electric field of frequency f was modeled by an $R||C$ circuit in the 0.1 Hz−1 MHz frequency range and at relatively low electric fields, E ($E_{\text{peak-to-peak}} < 1$ kV/cm). In this model the complex impedance Z is given by $Z = [R(1 - j\omega RC)]/(1 + (j\omega RC)^2)$, where R and C are the resistance and capacitance of the films, ω the pulsation ($\omega = 2\pi f$), and j the imaginary number. In this model, both parameters, R and C, are assumed independent of ω and $E_{\text{peak-to-peak}}$.

The determination of C for a given sample can be performed with very low error using impedance spectroscopy analysis from plots of the imaginary part of the admittance ($Y \equiv Z^{-1}$) as a function of ω. The $R||C$ model predicts $\text{Im}(Y) = -j\omega C$, that is, a linear response between $|\text{Im}(Y)|$ and ω. This linear relationship was already observed for all samples, as illustrated in Figure 3a. The values of C were recovered from the slope of plots $|\text{Im}(Y)|$ vs ω with high accuracy (0.2% for a single measurement and 20% for repetitions). In general, the obtained C fall in the range 1−20 pF, depending on W, $\langle L\rangle$, and the conditions of preparation (in absence or presence of E or H).

The capacitance, C, is given by $C = \varepsilon\varepsilon_0 a/\langle L\rangle$, where ε is the static dielectric constant, ε_0 is the vacuum permittivity, and a is the area of the top contact ($a = 0.01$ cm^2). Actually, Figure 3a shows plots of the modulus of the imaginary part of Y multiplied by $\langle L\rangle$ and divided by ε_0 and a as a function of ω; hence, the slope of the respective straight line in Figure 3a is equal to ε. The values of ε for samples **F-10**, **F-10E**, **F-10H**, **F50**, **F-50E**, and **F-50H**, represented as averages over several replicated samples, are presented in Figure 4 (indicating the standard deviations).

Impedance spectroscopy data for nonloaded SBR films were fitted with the $R||C$ model, obtaining $\varepsilon_{\text{SBR}} = 4 \pm 2$ (average obtained for several replicates; the error corresponds to their standard deviations). This value is in good agreement with values reported for SBR in the literature, although departures are expected due to factors such as the specific styrene/butadiene ratio, presence of additives, etc.[9] The dielectric constant of films prepared under the same preparation protocol increases with $BiFeO_3$ concentration, departing from the value ε_{SBR}.

It is worth noting that there is a large spread of reported values in the literature for the dielectric constant of $BiFeO_3$. For instance, values between 15 and 150 have been reported,[17,19−22] suggesting that ε of $BiFeO_3$ is highly sensitive to morphological parameters determined by synthesis, postsynthesis treatments, etc.

On the other hand, the usual way for obtaining the values of R is from plots of $|Z|$ vs ω in the limit of $\omega \to 0$. Large values of R, about 1−100 GΩ, were obtained. However, the accuracy of

DOI: 10.1021/acs.jpcc.5b06056
J. Phys. Chem. C XXXX, XXX, XXX−XXX

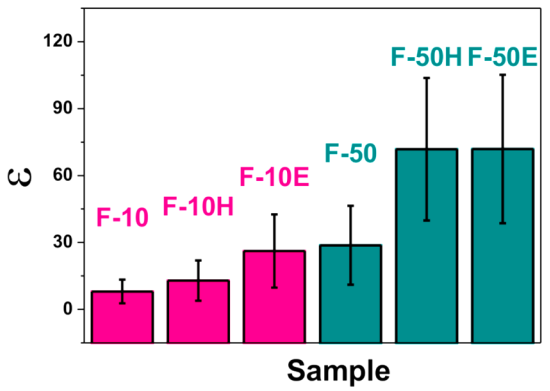

Figure 4. Relative dielectric constant, ε, for samples with W = 10 and 50, prepared in the presence/absence of electric and magnetic fields (E and H, respectively). The bars correspond to averages over several replicates (4−5). The errors are the standard deviation of those values.

those values was very low because the signals from impedance spectroscopy present large fluctuations (larger than 50%) at low frequencies for currents lower than nA, as in this case. Thus, determinations of the electrical resistivity, ρ, were performed by a different method (dc J−E plots, presented in section 3.5).

From Figure 4 it can be observed that samples with W = 50 present higher values of ε than those with W = 10. Additionally, we remark that samples of equal W but prepared under the application of a magnetic or electric field (samples **F-WH** and **F-WE**) show higher values of ε than samples **F-W**. These topics are discussed in the next section.

The dielectric losses are defined as $|\tan(\delta)| \equiv |\mathrm{Re}(Z)/\mathrm{Im}(Z)|$. The $R||C$ model predicts $|(\tan(\delta))^{-1}| RC(\omega)$. Figure 3b shows $|(\tan(\delta))^{-1}|$ vs ω. Although there is an important dispersion in the data, which comes from the large uncertainty in the real part of the impedance, $\mathrm{Re}(Z)$, it can be observed the increasing trend $|(\tan(\delta))^{-1}|$ with ω, in agreement with the prediction of the $R||C$ model.

3.3. Modeling ε as a Function of W. The dielectric constant was determined from impedance analysis as a function of W for films prepared in the absence and presence of H (Figure 5). In the case of films **F-WH**, the dielectric constant increases with W, but then saturation is observed (Figure 5b).

The increase of ε at low values of W (or the filler volume fraction, f^{vol}) has already reported for $BiFeO_3$ in different polymers.[15,23−26] Moreover, some authors found that the fast increase of ε is followed by a sudden decrease at larger concentrations.[13,23]

Effective medium field models seem to account for the rise of ε, at least qualitatively, but not for saturation at large concentrations and surely not for a decrease.[27−29] Thus, we propose a model to account for the dependence of ε as a function of W observed in our system.

The increase of ε at low W can be assigned to the simple fact that the total volume, which is initially only occupied by the polymer, is gradually occupied by the filler also. That is, the volume fraction of the filler increases, thus increasing the dielectric constant. In order to produce this increase, it is not necessary to have connection between filler agglomerates in the composite. It is just the gradual substitution of a poor dielectric polymer by good dielectric filler produces an increase of ε with filler concentration at low concentrations. This concept is the essence of effective medium models, and it seems to be a good description for samples prepared in the absence of H or E shown in Figure 5a. It also describes qualitatively well the behavior of ε at W < 20 for samples **F-WH** in Figure 5b. Note that the difference with respect to the case of increasing electrical conduction with filler concentration when using highly conductive fillers (like graphite, nickel, ruthenium dioxide, carbon nanotubes, etc.[30]) where percolation between agglomerates is required while here does not.

A further increase of concentration can drastically change the behavior. If particles are well dispersed (as in samples **F-WH** and **F-WE**), then electron transport mechanisms can occur between the several aggregates, and the films increase their electrical conduction, inducing relatively large leakage currents which opposes to improve the dielectric properties. In the cases reported by Bhadra et al.[13] and Dang et al.[23] the decrease of ε at the largest concentrations can be assigned to the presence of connectivity between aggregates that led to electrical conduction through the film (by any possible mechanism like tunneling or hopping). In our case we do not observe a decrease of ε with W but saturation (probably because leakage currents are lower in our system, as will be discussed in the next section).

Thus, it seems there are two regimes: one at low concentrations and other at higher concentrations. In the low concentrations regime ε increases with W because there is no relevant electrical conduction and the dielectric properties are improved by the partial and progressive replacement of the polymer matrix by the filler. On the other hand, connectivity seems to be present in the large filler concentration regime,

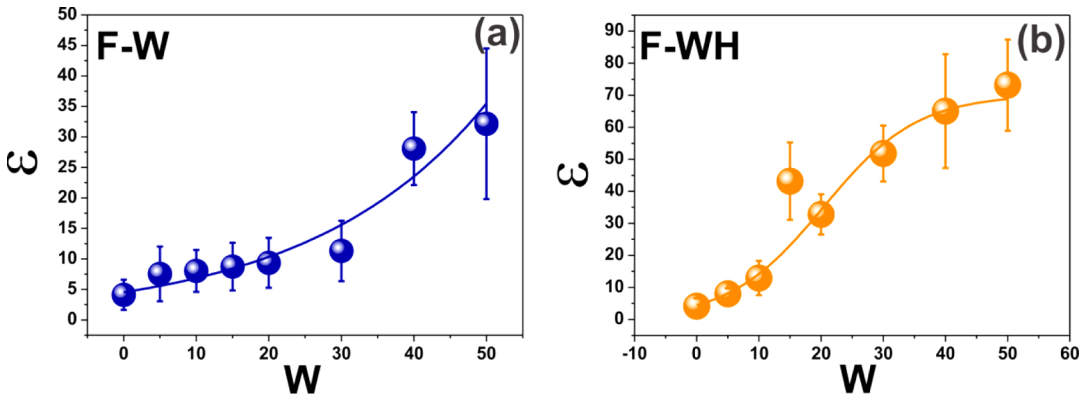

Figure 5. Dielectric constant, ε, as a function of $W = 100(M_{BiFeO_3}/M_{SBR})$. (a) Films **F-W**. (b) Films **F-WH**. The solid lines represent fits by eq 2.

DOI: 10.1021/acs.jpcc.5b06056
J. Phys. Chem. C XXXX, XXX, XXX−XXX

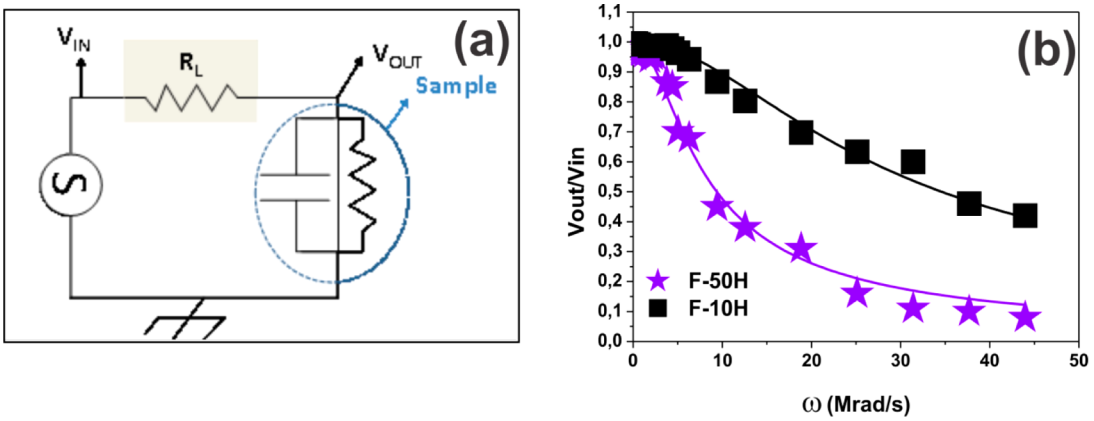

Figure 6. (a) Circuit used to study the film's response to sinusoidal excitations up to $f = 7$ MHz. (b) Ratio of the amplitudes (V_{OUT}/V_{IN}) vs ω: ■, **F-10H**; ★, **F-50H**. $R_L = 1$ kΩ.

increasing leakage currents which avoid a further increase of ε with concentration and reaching saturation. This description seems to be qualitatively in perfect agreement with the observations. The turnover between both regimes seems to appear at $W \cong 20-25$ by visual inspection in Figure 5a.

In order to present a quantitative description of the results presented in Figure 5, the experimental data of ε vs W were fitted by an expression that accounts well for experimental data where an exponential increase followed by inflection and saturation is observed.[31] It is assumed that any differential change of ε caused by differential changes in W is given by

$$d\varepsilon = \beta\varepsilon(\varepsilon_s - \varepsilon)dW \quad (1)$$

where β is a constant (β^{-1} has the same units as W) and ε_s is the dielectric constant at saturation. Integration of eq 1 under the boundary condition that $\varepsilon = \varepsilon_p$ at $W = 0$, where ε_p is the dielectric constant of the polymer matrix, provides the following expression for ε, used to fit the experimental data of Figure 5a,b:

$$\varepsilon = \varepsilon_s\left(\frac{1}{1 + \exp(-\beta(W - \mu))}\right) \quad (2)$$

where $\mu \equiv [\ln(\varepsilon_s - \varepsilon_p)/\varepsilon_s]/\beta$. The expression given by eq 2 has an inflection at $W = \mu$. Thus, μ provides an estimation of the turnover point for the regime change proposed in the proposed description: although the leakage currents may remain low enough to allow the system to be used as a capacitor, the rate at which ε varies with W, $d\varepsilon/dW$, decreases for $W > \mu$.

Fits of data points are reasonable good, as shown in Figure 5a,b. The parameters ε_p, ε_s, and β of eq 2 were considered as freely adjustable parameters, recovered by the fitting.

In the case of films **F-WH** (Figure 5b), the recovered values are $\varepsilon_p = 4 \pm 1$, $\varepsilon_s = 70 \pm 10$, and $\beta^{-1} = 8 \pm 1$. The recovered ε_p and ε_s are in excellent agreement with the experimental data measured at $W = 0$ ($\varepsilon_p = \varepsilon_{SBR}$) and at $W = 50$, respectively.

The calculated value of μ is 22 ± 4. The turnover volume fraction, $f^{vol}_{turnover}$, can be calculated as $f^{vol}_{turnover} = (\delta_{composite}/\delta_{BiFeO_3})[(\mu/100)/((\mu/100) + 1)]$ where the density of the inorganic agglomerates is assumed equal to the bulk density of $BiFeO_3$ ($\delta_{BiFeO_3} \cong 5$ g/cm^3, although dependent on crystallite size, structural defects, oxygen vacancies, etc.[32]). The density of the composites, $\delta_{composite}$, at $W = \mu$, were calculated by weighting and determination of its dimensions, obtaining $\delta_{composite} \cong 1.4$ g/cm^3. Then using $\mu = 22$ renders $f^{vol}_{turnover} \cong 0.05$ for samples **F-WH**. That is, the turnover is predicted at volume fractions about 5% for samples **F-WH**. Saturation is reached for $W = 50$, which corresponds to volume fractions about $f^{vol} \cong 0.09$ (9%).

For films **F-W** it was recovered $\beta^{-1} = 24 \pm 3$ and $\varepsilon_p = 4.5 \pm 0.8$. The value of ε_s was estimated larger than 100 with 100% error, which is reasonable since the experimental data points do not reach saturation (Figure 5a). Note that in both cases **F-W** and **F-WH**, the recovered values of ε_p are in very good agreement with the reported dielectric constant of SBR.[30,33]

Summarizing, preparation in the presence of magnetic fields induces larger values of the dielectric constant of the composite with respect to the polymer, in comparison with films prepared in its absence. There is another interesting characteristics of films prepared in the presence of magnetic fields, which is that although there is regime's turnover starting at $f^{vol} = 5\%$ ($W = \mu = 22$) that avoid a further increase of ε with filler concentration for $f^{vol} > 9\%$ ($W = 50$), the dielectric constant does not decrease but reaches saturation. This seems related to the fact that leakage currents remains limited in our system as will be shown in the next section.

3.4. Incorporation of the Films as Electric Components in an AC Circuit. After characterizing the ac properties of the films, we test them as capacitors in a real circuit, even at frequencies f a little higher than those used in the previous sections. The electric circuit shown in Figure 6a was used to determine the response of the samples to a sinusoidal excitation in an extended frequency range, up to $f = 7$ MHz. The electrical field was kept relatively low ($E < 1$ kV/cm) which for our samples correspond to peak-to-peak voltages lower than 10 V, similar to the voltages used in section 3.2.

The incorporation of the films as a component of a circuit allows illustrating the possibilities of the structured elastomeric composites as capacitors for concrete applications. The input voltage is given by $V_{IN}(t) = V^{pp}_{IN}\sin(\omega t)$. The output voltage, $V_{OUT}(t) = V^{pp}_{OUT}(\omega)\sin(\omega t + \varphi)$ (Figure 6a) was measured with a digital oscilloscope (see Experimental Section). V^{pp}_{OUT} and the phase φ are dependent on V^{pp}_{IN} and ω. Figure 6b show the experimental data of V^{pp}_{OUT}/V^{pp}_{IN} as a function of ω for the case of samples **F-10H** and **F-50H**. The solid lines in Figure 6b correspond to fits of the experimental points by a model that assumes the samples represented by an $R||C$ circuit with resistance and capacity values independent of ω. The recovered capacities are in the range 1−20 pF, in excellent agreement with the values obtained from impedance spectroscopy. Hence, the

DOI: 10.1021/acs.jpcc.5b06056
J. Phys. Chem. C XXXX, XXX, XXX−XXX

new values of ε, recovered by the present method and for f between 100 kHz and 7 MHz, are very similar to those obtained by impedance spectroscopy for frequencies f lower than 1 MHz reported in section 3.2 (Figures 4 and 5). For instance, the values $C = 16 \pm 3$ pF and $R = 3.0 \pm 0.6$ GΩ were obtained from the fits of Figure 6b for a sample **F-50H**. Thus, the results obtained from this method and impedance spectroscopy are consistent.

The recovered values of ρ recovered by the present method are in the order of 10−100 GΩ·cm. To confirm these values, dc density current (J) versus electric field (E) studies were recorded (see next section) in order to obtain reliable estimations of ρ and to accurately evaluate the leakage currents.

3.5. DC *J*–*E* Plots (Leakage Currents). Examples of the dc density current, J, for several samples, as a function of the applied electric field, E, are shown in Figure 7 (J–E plots).

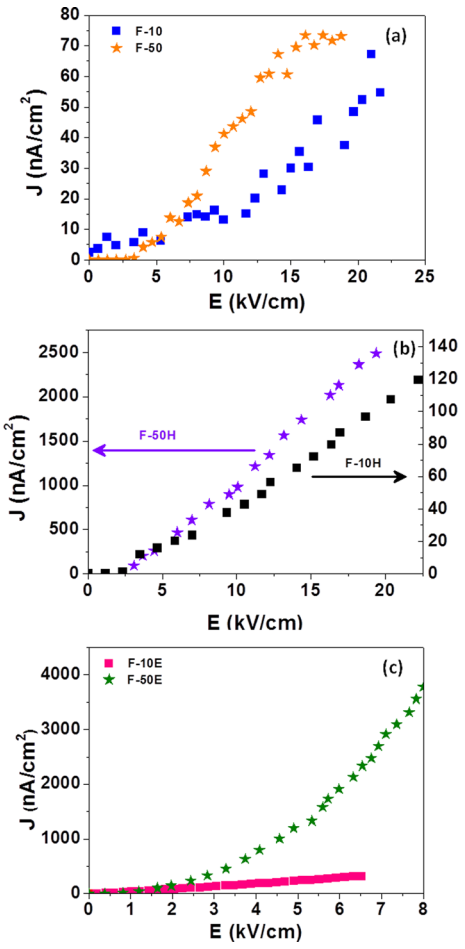

Figure 7. Plot of dc density current (J) vs electric field (E). (a) **F-10** and **F-50**. (b) **F-10H** and **F-50H**. (c) **F-10E** and **F-50E**.

The plots of Figure 7 were registered under positive bias (the n-Si substrate connected to ground and the top electrode to a positive potential). The current densities under negative bias (negative biased top electrode) are slightly lower; the difference can be assigned to the different barriers on the electrode/multiferroic composite interfaces, as well reported in the literature.[34,35] Values of the electrical resistivity, ρ, for each SBR/$BiFeO_3$ film were obtained from the inverse of the J–E slopes. The values are in the order of 1−200 GΩ·cm, much higher than those of pure $BiFeO_3$ films or compressed $BiFeO_3$ pellets which are about 1−10 MΩ cm.[17]

Although a systematic concentration scan of ρ as a function of W was not performed, the observed trend in the composites is that ρ for $W = 50$ is much lower than for $W = 10$, at a given preparation protocol. Additionally, at $W = 50$, ρ is much lower for samples prepared in the presence of the fields E or H: ρ(**F-50**) ≫ ρ(**F-50E**), ρ(**F-50H**). For instance, for the case of samples shown in Figure 7a,b, it was obtained ρ(**F-10**) ≅ 400 GΩ·cm, ρ(**F-10H**) ≅ 100 GΩ·cm, ρ(**F-50**) ≅ 250 GΩ·cm, and ρ(**F-50H**) ≅ 10 GΩ·cm. These values are in agreement with those obtained in the previous sections using different methods. Similar trends hold when comparing samples **F-W** and **F-WE** (e.g., comparing Figures 7a and 7c).

For films **F-WH** the resistivities are in the order of 10^2 GΩ·cm for $W < \mu$, similar to those reported for PVDF/$BiFeO_3$ composites by Bhadra et al.[13] However, in the present case, the decrease of ρ for $W > \mu$ is not larger than 1 order of magnitude (for example, ρ(**F-10H**) ≅ 100 GΩ·cm and ρ(**F-50H**) ≅ 10 GΩ·cm). This is a significant difference with respect to the mentioned work, where a decrease of ρ about 3−4 orders of magnitude was reported above the turnover, with the correspondent increase of the leakage currents in similar orders.

Thus, in the present work the leakage currents above the concentration's turnover are limited to 1−10 of its values below the turnover.

3.6. Electric Polarization Curves and Magnetoelectric Coupling. The films **F-10**, **F-10H**, and **F-10E** have very small values of dielectric polarization in comparison with those of **F-50E** and **F-50H** (about 1 order of magnitude lower, not shown), without observing appreciable magnetoelectric coupling at room temperature. The following analysis corresponds to films **F-50H** only. Electric polarization curves of a **F-50H** film are shown in Figure 8a.

These curves are representative of the dependence of the dielectric polarization, P, with an applied electric field, E (dc), referred as P–E plots. All **F-50H** films presented electric hysteresis, assigned to the well-known ferroelectric behavior of the $BiFeO_3$ ceramics. The different plots in Figure 8a correspond to P–E curves that were scanned in the presence of different magnetic field, H, applied on the already prepared films. Note that the field H shown in Figure 8 is not the field used to prepare the films, which was always 360 mT. This field H is the magnetic field applied on the films **F-50H** when recording the P–E curves.

The scanned electric fields in the P–E curves are limited to a range allowed by the instrumentation (±10 kV/cm). In that range, no saturation of the polarization is reached. As a consequence, the maximum polarization value does not correspond to saturation of the dielectric response, a well-known effect.[36] Moreover, a polarization downturn is observed for higher electrical fields. This is likely an artifact related to the presence of leakage currents in the capacitor.[37] Therefore, the P–E plots shown in Figure 8a must be taken only as an indication of the ferroelectric nature of the composites and of the relative variation of the P–E curves with H, but not as representative of quantitative values of P. For this reason, the curves recorded for different values of H are presented as normalized values to the value at $E = 0$ for the curve registered in the absence of magnetic field (a relative value of polarization equal to 100 is arbitrarily assigned to the point at $E = 0$ in the curve of $H = 0$). Similar electric polarization curves, showing no saturation and increasing of the electric polarization when

DOI: 10.1021/acs.jpcc.5b06056
J. Phys. Chem. C XXXX, XXX, XXX−XXX

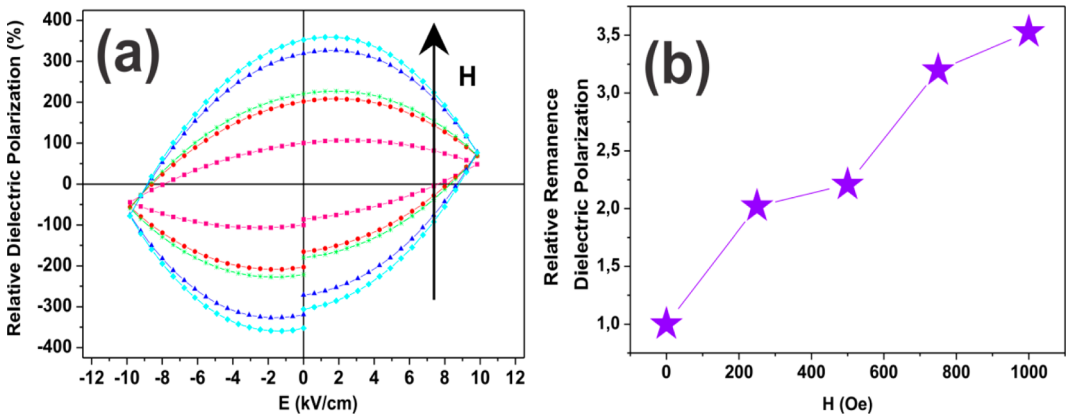

Figure 8. (a) Relative dielectric polarization vs electric field (E) for films **F-50H**, measured in the presence of an external a magnetic field, H: ■, 0 Oe; ●, 250 Oe; ∗, 500 Oe; ▲, 750 Oe; ◆, 1000 Oe. (b) Relative changes of the observed remanence polarization as a function of H (film: **F-50H**).

applying magnetic fields, were also observed by Sadhana et al.[38] in a complex mixture of doped $BaTiO_3$ and $ZnFe_2O_4$ nanocomposites. Yao et al.[39] have also found nonsaturated electric polarization curves for $BiFeO_3$−$BaTiO_3$ bulk composites sintered under oxygen atmosphere, with similar values of resistivity as those reported in this paper.

Figure 8a shows that films **F-50H** present a magnetoelectric coupling at room temperature, given by the increase of P−E curves with H. At fields higher than 1000 Oe, the signals increases above the limit allowed by instrumentation factors and no further changes were allowed to be accurately measured.

The relative changes of the remanence polarization with H, below 1000 Oe, are presented in Figure 8b, where $P(E = 0, H)/P(E = 0, H = 0)$ as a function of H is represented for films **F-50H**. It is observed an increment of 3.5 times when samples are under a magnetic field of 1000 Oe in comparison with the case $H = 0$. As $BiFeO_3$ is a multiferroic compound that presents a "positive" electromagnetic coupling,[40] $(\partial P/\partial H)_E > 0$; hence, the observed increase of the relative polarization with H (Figure 8b) is in agreement with the expected behavior for $BiFeO_3$.

The observed dependence of the relative remanence with H is approximately linear in the considered range, with a variation rate about 3.5×10^{-3} Oe^{-1}. In principle, that value can be compared with estimations of $1/P_{rem}(\partial P/\partial H)_{E=0}$, using reported values, where P_{rem} is the remanence polarization, $P_{rem} = P(E = 0, H = 0)$. However, the spread of reported values is very large, as shown in the following discussion. For the first factor, P_{rem}, values in the range 0.1−20 $\mu C\ cm^{-2}$ have been reported for $BiFeO_3$ bulk.[41−48] The other factor, $(\partial P/\partial H)_{E=0}$, can be taken equal to the product of two other factors: $[(\partial P/\partial H)_{E=0}][(\partial P/\partial H)_{E=0}]$. These two last factors can be obtained from literature, but a large diversity of values are found, dependent on the type of samples (e.g., films or pellets), synthesis conditions, Bi substitution, etc. The first factor, $[(\partial P/\partial H)_{E=0}]$, must be taken from P−E curves where saturation is reached (the factor is equal to the slope of the P−E curves at $E = 0$ in those plots), presenting reported values in the range 10^{-4}−10^{-1} $\mu CV^{-1}\ cm^{-1}$.[41,44,49] In the case of the second factor, $[(\partial P/\partial H)_{E=0}]$, which is usually referred as the *electromagnetic coupling*, a range of values have been reported from 10^{-1} V cm^{-1} Oe^{-1} up to 12 V cm^{-1} Oe^{-1}.[40,50] Considering these values, the possibilities for $(1/P_{rem})(\partial P/\partial H)_{E=0}$ are very large, estimating a range between 10^{-7}−10^{2} Oe^{-1}. The slope from Figure 8b, 3.5×10^{-3} Oe^{-1}, falls about in the middle of that range, not surprising considering the large spread of reported values.

4. CONCLUSIONS

The application of electric or magnetic fields during preparation constitutes a significant improvement for using elastomer/$BiFeO_3$ in electronics. These composites can be used as capacitive components in electrical circuits, displaying low leakage currents. Preliminary evidence of magnetoelectric coupling, with a strong dependence of the dielectric polarization curves with magnetic fields applied after preparation was found. Thus, a ferroelectric polymer is not an imperative requisite in order to obtain elastic capacitors with remarkable features. The key factor seems to be the improvement in the dispersion of $BiFeO_3$ a driven by the fields applied during preparation.

■ AUTHOR INFORMATION

Corresponding Author

*E-mail rmn@qi.fcen.uba.ar; Tel +54-11-4576-3358; Fax +54-11-4576-3341 (R.M.N.).

Notes

The authors declare no competing financial interest.

G.A.J.: On leave from Laboratorio de Bajas Temperaturas, Facultad de Ciencias Exactas y Naturales, Universidad de Buenos Aires, Argentina.

■ ACKNOWLEDGMENTS

D.R., G.J., N.D., and R.M.N. are research members of the National Council of Research and Technology (CONICET, Argentina). L.M.S.M. is a PhD student at the University of Buenos Aires (UBA) with a doctoral fellowship from CONICET. Financial support was received from UBA (UBACyT 2012-2015, projects 2002 01101 00098, 2002 201001 00142 and UBACyT 2014-2017, 20020130100021BA), Ministry of Science, Technology and Innovations (MINCYT-FONCYT, Argentina, PICT 2011-0377 and PICT-2012-0717), CONICET, and CIC-Buenos Aires (PIP-Conicet 0291 and PIP 2014-2016, 112-201101-00370CO). The authors thank Dr. Angel Marzocca (FATE S.A.I.C., Argentina) for providing the SBR. The Laboratorio de Bajas Temperaturas is acknowledged (School of Sciences, UBA) for facilities concerning magnetic measurements. The Center of Advanced Microscopy (CMA), UBA, is acknowledged for the SEM-AFM images. The authors thank Dr. César

DOI: 10.1021/acs.jpcc.5b06056
J. Phys. Chem. C XXXX, XXX, XXX−XXX

Barbero (Universidad Nacional de Río Cuarto, Argentina) for helpful discussions and providing his insights concerning the physics associated with the dependence of ε with the filler's volume fraction.

REFERENCES

(1) Høyer, H.; Knaapila, M.; Kjelstrup-Hansen, J.; Helgesen, G. Microelectromechanical Strain and Pressure Sensors Based on Electric Field Aligned Carbon Cone and Carbon Black Particles in a Silicone Elastomer Matrix. *J. Appl. Phys.* **2012**, *112*, 094324.

(2) Ausanio, G.; Iannotti, V.; Ricciardi, E.; Lanotte, L.; Lanotte, L. Magneto-Piezoresistance in Magnetorheological Elastomers for Magnetic Induction Gradient or Position Sensors. *Sens. Actuators, A* **2014**, *205*, 235−239.

(3) Mietta, J. L.; Jorge, G.; Perez, O. E.; Maeder, T.; Negri, R. M. Superparamagnetic Anisotropic Elastomer Connectors Exhibiting Reversible Magneto-Piezoresistivity. *Sens. Actuators, A* **2013**, *192*, 34−41.

(4) Vacca, P.; Nenna, G.; Miscioscia, R.; Palumbo, D.; Minarini, C.; Sala, D. D. Patterned Organic and Inorganic Composites for Electronic Applications. *J. Phys. Chem. C* **2009**, *113*, 5777−5783.

(5) Kohlmeyer, R. R.; Javadi, A.; Pradhan, B.; Pilla, S.; Setyowati, K.; Chen, J.; Gong, S. Electrical and Dielectric Properties of Hydroxylated Carbon Nanotube−Elastomer Composites. *J. Phys. Chem. C* **2009**, *113*, 17626−17629.

(6) Park, S.; Vosguerichian, M.; Bao, Z. A Review of Fabrication and Applications of Carbon Nanotube Film-Based Flexible Electronics. *Nanoscale* **2013**, *5*, 1727−1752.

(7) Mietta, J. L.; Ruiz, M. M.; Antonel, P. S.; Perez, O. E.; Butera, A.; Jorge, G.; Negri, R. M. Anisotropic Magnetoresistance and Piezoresistivity in Structured Fe_3O_4-Silver Particles in PDMS Elastomers at Room Temperature. *Langmuir* **2012**, *28*, 6985−6996.

(8) Mietta, J. L.; Jorge, G.; Martín Negri, R. A Flexible Strain Gauge Exhibiting Reversible Piezoresistivity Based on an Anisotropic Magnetorheological Polymer. *Smart Mater. Struct.* **2014**, *23*, 085026.

(9) Ruiz, M. M.; Claudia Marchi, M.; Perez, O. E.; Jorge, G. E.; Fascio, M.; D'Accorso, N.; Martín Negri, R. Structured Elastomeric Submillimeter Films Displaying Magneto and Piezo Resistivity. *J. Polym. Sci., Part B: Polym. Phys.* **2015**, *53*, 574−586.

(10) Lekha, C.; Sudarsanan, V.; Pookat, G. Spintronic Devices Based on Multiferroics, A Review of Patents. *Recent Pat. Mater. Sci.* **2014**, *7*, 103−108.

(11) Mandal, B. P.; Vasundhara, K.; Abdelhamid, E.; Lawes, G.; Salunke, H. G.; Tyagi, A. K. Improvement of Magnetodielectric Coupling by Surface Functionalization of Nickel Nanoparticles in Ni and Polyvinylidene Fluoride Nanohybrids. *J. Phys. Chem. C* **2014**, *118*, 20819−20825.

(12) Qin, W.; Jasion, D.; Chen, X.; Wuttig, M.; Ren, S. Charge-Transfer Magnetoelectrics of Polymeric Multiferroics. *ACS Nano* **2014**, *8*, 3671−3677.

(13) Bhadra, D.; Masud, M. G.; Sarkar, S.; Sannigrahi, J.; De, S. K.; Chaudhuri, B. K. Synthesis of PVDF/$BiFeO_3$ Nanocomposite and Observation of Enhanced Electrical Conductivity and Low-Loss Dielectric Permittivity at Percolation Threshold. *J. Polym. Sci., Part B: Polym. Phys.* **2012**, *50*, 572−579.

(14) Tamboli, M. S.; Palei, P. K.; Patil, S. S.; Kulkarni, M. V.; Maldar, N. N.; Kale, B. B. Polymethyl Methacrylate (PMMA)-Bismuth Ferrite (BFO) Nanocomposite: Low Loss and High Dielectric Constant Materials with Perceptible Magnetic Properties. *Dalton Trans.* **2014**, *43*, 13232−13241.

(15) Ahlawat, A.; Satapathy, S.; Bhartiya, S.; Singh, M. K.; Choudhary, R. J.; Gupta, P. K. $BiFeO_3$/poly(methyl methacrylate) Nanocomposite Films: A Study on Magnetic and Dielectric Properties. *Appl. Phys. Lett.* **2014**, *104*, 042902.

(16) Catalan, G.; Scott, J. F. Physics and Applications of Bismuth Ferrite. *Adv. Mater.* **2009**, *21*, 2463−2485.

(17) Saleh Medina, L. M.; Jorge, G. A.; Negri, R. M. Structural, Dielectric and Magnetic Properties of $Bi_{1-x}Y_xFeO_3$ Obtained by Acid−Base Co-Precipitation. *J. Alloys Compd.* **2014**, *592*, 306−312.

(18) De Falco, A.; Lamanna, M.; Goyanes, S.; D'Accorso, N. B.; Fascio, M. L. Thermomechanical Behavior of SBR Reinforced with Nanotubes Functionalized with Polyvinylpyridine. *Phys. B* **2012**, *407*, 3175−3177.

(19) Cui, Y. F.; Zhao, Y. G.; Luo, L. B.; Yang, J. J.; Chang, H.; Zhu, M. H.; Xie, D.; Ren, T. L. Dielectric, Magnetic, and Magnetoelectric Properties of La and Ti Codoped $BiFeO_3$. *Appl. Phys. Lett.* **2010**, *97*, 222904.

(20) Chen, X.-Z.; Yang, R.-L.; Zhou, J.-P.; Chen, X.-M.; Jiang, Q.; Liu, P. Dielectric and Magnetic Properties of Multiferroic $BiFeO_3$ Ceramics Sintered with the Powders Prepared by Hydrothermal Method. *Solid State Sci.* **2013**, *19*, 117−121.

(21) Song, G. L.; Zhang, H. X.; Wang, T. X.; Yang, H. .; Chang, F. G. Effect of Sm, Co Codoping on the Dielectric and Magnetoelectric Properties of $BiFeO_3$ Polycrystalline Ceramics. *J. Magn. Magn. Mater.* **2012**, *324*, 2121−2126.

(22) Kumar, P.; Kar, M. Effect of Structural Transition on Magnetic and Dielectric Properties of La and Mn Co-Substituted $BiFeO_3$ Ceramics. *Mater. Chem. Phys.* **2014**, *148*, 968−977.

(23) Dang, Y.; Wang, Y.; Deng, Y.; Li, M.; Zhang, Y.; Zhang, Z. Enhanced Dielectric Properties of Polypropylene Based Composite Using Bi_2S_3 Nanorod Filler. *Prog. Nat. Sci.* **2011**, *21*, 216−220.

(24) Pecharromán, C.; Esteban-Betegón, F.; Bartolomé, J. F.; López-Esteban, S.; Moya, J. S. New Percolative $BaTiO_3$−Ni Composites with a High and Frequency-Independent Dielectric Constant ($\epsilon r \approx 80000$). *Adv. Mater.* **2001**, *13*, 1541−1544.

(25) Huang, C.; Zhang, Q. M.; deBotton, G.; Bhattacharya, K. All-Organic Dielectric-Percolative Three-Component Composite Materials with High Electromechanical Response. *Appl. Phys. Lett.* **2004**, *84*, 4391−4393.

(26) Huang, C.; Zhang, Q. M.; Li, J. Y.; Rabeony, M. Colossal Dielectric and Electromechanical Responses in Self-Assembled Polymeric Nanocomposites. *Appl. Phys. Lett.* **2005**, *87*, 182901.

(27) Patil, S. K.; Koledintseva, M.; Schwartz, R. W.; Huebner, W. Prediction of Effective Permittivity of Diphasic Dielectrics Using an Equivalent Capacitance Model. *J. Appl. Phys.* **2008**, *104*, 074108.

(28) Barber, P.; Balasubramanian, S.; Anguchamy, Y.; Gong, S.; Wibowo, A.; Gao, H.; Ploehn, H. J.; Zur Loye, H.-C. Polymer Composite and Nanocomposite Dielectric Materials for Pulse Power Energy Storage. *Materials* **2009**, *2*, 1697−1733.

(29) Wu, Y.; Zhao, X.; Li, F.; Fan, Z. Evaluation of Mixing Rules for Dielectric Constants of Composite Dielectrics by MC-FEM Calculation on 3D Cubic Lattice. *J. Electroceram.* **2003**, *11*, 227−239.

(30) Karásek, L.; Meissner, B.; Asai, S.; Sumita, M. Percolation Concept: Polymer-Filler Gel Formation, Electrical Conductivity and Dynamic Electrical Properties of Carbon-Black-Filled Rubbers. *Polym. J.* **1996**, *28*, 121−126.

(31) Negri, R. M.; Rodriguez, S. D.; Bernik, D. L.; Molina, F. V.; Pilosof, A.; Perez, O. A Model for the Dependence of the Electrical Conductance with the Applied Stress in Insulating-Conducting Composites. *J. Appl. Phys.* **2010**, *107*, 113703.

(32) Martí, X.; Ferrer, P.; Herrero-Albillos, J.; Narvaez, J.; Holy, V.; Barrett, N.; Alexe, M.; Catalan, G. Skin Layer of $BiFeO_3$ Single Crystals. *Phys. Rev. Lett.* **2011**, *106*, 236101.

(33) Gunasekaran, S.; Natarajan, R.; Kala, A.; Jagannathan, R. Dielectric Studies of Some Rubber Materials at Microwave Frequencies. *Indian J. Pure Appl. Phys.* **2008**, *46*, 733−737.

(34) Xing, W.; Ma, Y.; Ma, Z.; Bai, Y.; Chen, J.; Zhao, S. Improved Ferroelectric and Leakage Current Properties of Er-Doped $BiFeO_3$ Thin Films Derived from Structural Transformation. *Smart Mater. Struct.* **2014**, *23*, 085030.

(35) Li, Y.-H.; Chen, F.; Gao, G.-Y.; Xu, H.-R.; Wu, W. Ferroelectric, Dielectric and Leakage Current Properties of Epitaxial (K,Na)NbO_3-$LiTaO_3$-$CaZrO_3$ Thin Films. *J. Electroceram.* **2015**, 1−6.

(36) Yan, H.; Inam, F.; Viola, G.; Ning, H.; Zhang, H.; Jiang, Q.; Zeng, T.; Gao, Z.; Reece, M. J. The Contribution of Electrical

DOI: 10.1021/acs.jpcc.5b06056
J. Phys. Chem. C XXXX, XXX, XXX−XXX

Conductivity, Dielectric Permittivity and Domain Switching in Ferroelectric Hysteresis Loops. *J. Adv. Dielectr.* **2011**, *1*, 107−118.
(37) Fina, I.; Fàbrega, L.; Langenberg, E.; Martí, X.; Sánchez, F.; Varela, M.; Fontcuberta, J. Nonferroelectric Contributions to the Hysteresis Cycles in Manganite Thin Films: A Comparative Study of Measurement Techniques. *J. Appl. Phys.* **2011**, *109*, 074105.
(38) Sadhana, K.; Ramana Murthy, S.; Jie, S.; Xie, Y.; Liu, Y.; Zhan, Q.; Li, R.-W. Magnetic Field Induced Polarization and Magnetoelectric Effect of $Ba_{0.8}Ca_{0.2}TiO_3$-$Ni_{0.2}Cu_{0.3}Zn_{0.5}Fe_2O_4$ Nanomultiferroic. *J. Appl. Phys.* **2013**, *113*, 17C731.
(39) Yao, Z.; Xu, C.; Liu, H.; Hao, H.; Cao, M.; Wang, Z.; Song, Z.; Hu, W.; Ullah, A. Greatly Reduced Leakage Current and Defect Mechanism in Atmosphere Sintered $BiFeO_3$−$BaTiO_3$ High Temperature Piezoceramics. *J. Mater. Sci.: Mater. Electron.* **2014**, *25*, 4975−4982.
(40) Costa, L. V.; Ranieri, M. G.; Cilense, M.; Longo, E.; Simoes, Z. Evidence of Magnetoelectric Coupling on Calcium Doped Bismuth Ferrite Thin Films Grown by Chemical Solution Deposition. *J. Appl. Phys.* **2014**, *115*, 17D910.
(41) Rojac, T.; Kosec, M.; Budic, B.; Setter, N.; Damjanovic, D. Strong Ferroelectric Domain-Wall Pinning in $BiFeO_3$ Ceramics. *J. Appl. Phys.* **2010**, *108*, 074107.
(42) Yu, B.; Li, M.; Wang, J.; Pei, L.; Guo, D.; Zhao, X. Enhanced Electrical Properties in Multiferroic $BiFeO_3$ Ceramics Co-Doped by La^{3+} and V^{5+}. *J. Phys. D: Appl. Phys.* **2008**, *41*, 185401.
(43) Chen, F.; Zhang, Q. F.; Li, J. H.; Qi, Y. J.; Lu, C. J.; Chen, X. B.; Ren, X. M.; Zhao, Y. Sol-Gel Derived Multiferroic $BiFeO_3$ Ceramics with Large Polarization and Weak Ferromagnetism. *Appl. Phys. Lett.* **2006**, *89*, 092910.
(44) Zhang, S. T.; Lu, M. H.; Wu, D.; Chen, Y. F.; Ming, N. B. Larger Polarization and Weak Ferromagnetism in Quenched $BiFeO_3$ Ceramics with a Distorted Rhombohedral Crystal Structure. *Appl. Phys. Lett.* **2005**, *87*, 262907.
(45) Das, S. R.; Choudhary, R. N. P.; Bhattacharya, P.; Katiyar, R. S.; Dutta, P.; Manivannan, A.; Seehra, M. S. Structural and Multiferroic Properties of La-Modified BiFeO3 Ceramics. *J. Appl. Phys.* **2007**, *101*, 034104.
(46) Wang, Y.; Zhou, L.; Zhang, M.; Chen, X.; Liu, J.-M.; Liu, Z. Room-Temperature Saturated Ferroelectric Polarization in $BiFeO_3$ Ceramics Synthesized by Rapid Liquid Phase Sintering. *Appl. Phys. Lett.* **2004**, *84*, 1731−1733.
(47) Arya, G. S.; Negi, N. S. Effect of In and Mn Co-Doping on Structural, Magnetic and Dielectric Properties of $BiFeO_3$ Nanoparticles. *J. Phys. D: Appl. Phys.* **2013**, *46*, 095004.
(48) Ramana, E. V.; Mahajan, A.; Graça, M. P. F.; Srinivas, A.; Valente, M. A. Ferroelectric and Magnetic Properties of Magnetoelectric $(Na_{0.5}Bi_{0.5})TiO_3$−$BiFeO_3$ Synthesized by Acetic Acid Assisted Sol−gel Method. *J. Eur. Ceram. Soc.* **2014**, *34*, 4201−4211.
(49) Palkar, V. R.; Kundaliya, D. C.; Malik, S. K.; Bhattacharya, S. Magnetoelectricity at Room Temperature in the $Bi_{0.9-x}Tb_xLa_{0.1}FeO_3$ System. *Phys. Rev. B: Condens. Matter Mater. Phys.* **2004**, *69*, 212102.
(50) Caicedo, J. M.; Zapata, J. A.; Gómez, M. E.; Prieto, P. Magnetoelectric Coefficient in $BiFeO_3$ Compounds. *J. Appl. Phys.* **2008**, *103*, 07E306.

DOI: 10.1021/acs.jpcc.5b06056
J. Phys. Chem. C XXXX, XXX, XXX−XXX